Electronic Structure of Ferromagnetic Semiconductor $Ga_{1-x}Mn_xAs$ Probed by Subgap Magneto-optical Spectroscopy

G. Acbas,[1] M.-H. Kim,[1] M. Cukr,[2] V. Novák,[2] M. A. Scarpulla,[3] O. D. Dubon,[3] T. Jungwirth,[2,4] Jairo Sinova,[5,2] and J. Cerne[1]

[1]*Department of Physics, University at Buffalo, SUNY, Buffalo, New York 14260, USA*
[2]*Institute of Physics ASCR, v.v.i., Cukrovarnick 10, 162 53 Praha 6, Czech Republic*
[3]*Department of Materials Science and Engineering and Lawrence Berkeley National Laboratory, University of California, Berkeley, California 94720, USA*
[4]*School of Physics and Astronomy, University of Nottingham, Nottingham NG7 2RD, United Kingdom*
[5]*Department of Physics, Texas A&M University, College Station, Texas 77843-4242, USA*

(Received 1 July 2009; published 24 September 2009)

We employ Faraday and Kerr effect spectroscopy in the infrared range to investigate the electronic structure of $Ga_{1-x}Mn_xAs$ near the Fermi energy. The band structure of this archetypical dilute-moment ferromagnetic semiconductor has been a matter of controversy, fueled partly by previous measurements of the unpolarized infrared absorption and their phenomenological impurity-band interpretation. Unlike the unpolarized absorption, the infrared magneto-optical effects we study are intimately related to ferromagnetism, and their interpretation is much more microscopically constrained in terms of the orbital character of the relevant band states. We show that the conventional theory of the disordered valence band with an antiferromatnetic exchange term accounts semiquantitatively for the overall characteristics of the measured infrared magneto-optical spectra.

DOI: 10.1103/PhysRevLett.103.137201 PACS numbers: 75.50.Pp, 71.55.Eq, 78.20.Ls, 78.66.Fd

The study of diluted magnetic semiconductors based on III-V compounds, in particular, $Ga_{1-x}Mn_xAs$, has been a very active area of research over the past two decades ever since the discovery of carrier mediated ferromagnetism in these materials [1]. $Ga_{1-x}Mn_xAs$ can exhibit metallic as well as insulating behavior depending on the doping and growth procedures, with the onset of ferromagnetism occurring near the insulator-to-metal transition. The perception that this transition occurs in a disordered valence band as in conventional *p*-doped semiconductors [2–5] and that many of the key magnetic properties are reminiscent of common itinerant ferromagnets [6,7] makes $Ga_{1-x}Mn_xAs$ an archetypical ferromagnetic semiconductor system. The notion has inspired numerous studies that contributed to our understanding of basic magnetic and magnetotransport properties of diluted magnetic semiconductors and led to discoveries of new effects and device concepts, including various types of spintronic transistors [8]. Nevertheless, the character of states near the Fermi energy in ferromagnetic $Ga_{1-x}Mn_xAs$ is still a matter of controversy [9–15] fueled in part by phenomenological interpretations of optical spectroscopy studies [9,14,15] which are inconsistent with the conventional semiconductor valence-band picture of the material.

A single broad peak at ~200 meV observed in unpolarized infrared absorption spectra has been interpreted by placing the Fermi energy in a narrow impurity band detached from the semiconductor valence band, which persists on the metallic side of the transition [9]. Competing with this phenomenological picture, a semiquantitative agreement with the experimental peak position and magnitude of the absorption has been obtained from microscopic calculations based on the disordered valence-band theory and considering transitions within the valence band [10]. The merit of the infrared spectroscopy is that it probes electronic states near the Fermi energy. The unpolarized absorption spectra, however, do not distinguish between transitions originating from states corresponding to intrinsic $Ga_{1-x}Mn_xAs$ and from extrinsic impurities, and do not provide specific information on the magnetic and orbital character of states involved in the optical transitions. A quantitative microscopic modeling of these spectra is complicated by the relatively strong intentional and unintentional disorder in these heavily doped semiconductors and by the vicinity of the metal-insulator transition [10]. Without microscopic modeling, the absence of a direct link between the measured spectra and the exchange-split and spin-orbit coupled electronic states leaves a relatively unconstrained space for inferring phenomenological pictures of the underlying band structure.

In this Letter we present results of Faraday and Kerr measurements in the mid- and near-infrared spectral range (115–1300 meV) for several ferromagnetic $Ga_{1-x}Mn_xAs$ samples grown by low temperature molecular beam epitaxy [16] and a sample grown by a combination of ion implantation and laser pulsed melting [17,18]. Our work complements previously reported higher energy (starting from 600 meV) magneto-optical measurements in $Ga_{1-x}Mn_xAs$ [15,19–25] (the magnetic circular dichroism is twice the Faraday ellipticity). The interpretation of these higher energy spectra is complicated by the fact that they are sensitive to many desired as well as undesired transi-

tions near the host semiconductor absorption edge. The infrared magneto-optical data studied here provide a unique probe into the nature of electronic states near the Fermi level. In contrast to the unpolarized absorption which is proportional to the longitudinal conductivity, the Faraday and Kerr effects arise from the transverse conductivity. Therefore Faraday and Kerr measurements are sensitive to the difference in the sample's response to left and right circularly polarized light, while unpolarized absorbtion spectra are related to the sum. The Faraday and Kerr effects represent a finite frequency analogue of the anomalous Hall effect with which they share the common exchange-splitting and spin-orbit coupling origin. The anomalous Hall effect has been described microscopically on a semiquantitative level using the conventional semiconductor valence-band theory [26]. Here we show that by extending the same microscopic theory to finite frequencies we capture key characteristics of the measured infrared magneto-optical spectra, again on a semiquantitative level, as predicted by early theory studies [27,28]. We have not performed alternative calculations that would correspond to any of the phenomenological variants of the impurity-band model. For calculating the transverse conductivity one has to specify the microscopic spin and orbital character of the relevant states. As explained in detail elsewhere [29], we have not found any microscopic representation that yields a detached impurity band in ferromagnetic $Ga_{1-x}Mn_xAs$ materials.

The measurements were performed with a polarization modulation technique using various gas and semiconductor laser sources, as well as a custom-modified double pass prism monochromator with a Xe light source. For details of the experimental technique see Refs. [30–32]. The method was tested by studying semiconductor materials with known behavior in the mid- and near-infrared range [32]. The magnetic field dependence of the complex Faraday θ_F and Kerr θ_K angles is measured at each wavelength and various temperatures from 6 to 300 K. At temperatures below T_c the magnetic field dependence of the rotation $\mathrm{Re}(\theta)$ and ellipticity $\mathrm{Im}(\theta)$ exhibits a saturation behavior due to alignment of the magnetization with the external field perpendicular to the sample surface. The behavior is superimposed on a linear dependence at a higher field due to the response of the wedged GaAs substrate, the $Ga_{1-x}Mn_xAs$ film, and the cryostat windows (see inset in Fig. 1). We subtract the linear component and record the rotation and ellipticity signals corresponding to saturation magnetization. In principle, this may not completely remove the paramagnetic contribution, but this contribution is an order of magnitude weaker than the ferromagnetic one in this spectral range and is generally represented by a Brillouin function of the external magnetic field and temperature. For our measurements (at temperatures above 10 K and magnetic fields below 1.5 T), the paramagnetic signal is linear in the magnetic field. Since the Faraday (Kerr) signal [30,31] is normalized by the total intensity of the transmitted (reflected) light, strong spectral features in the transmittance (reflectance) of the paramagnetic regions could produce artifacts in the Faraday (Kerr) signal. We may expect the contribution to the total transmission (reflection) of light through (from) paramagnetic regions to slightly shift the absolute value of θ_F (θ_K). However, since the measured transmittance (reflectance) varies slowly in the mid- and near-infrared range, these spectral artifacts in θ_F (θ_K) are expected to play a negligible role.

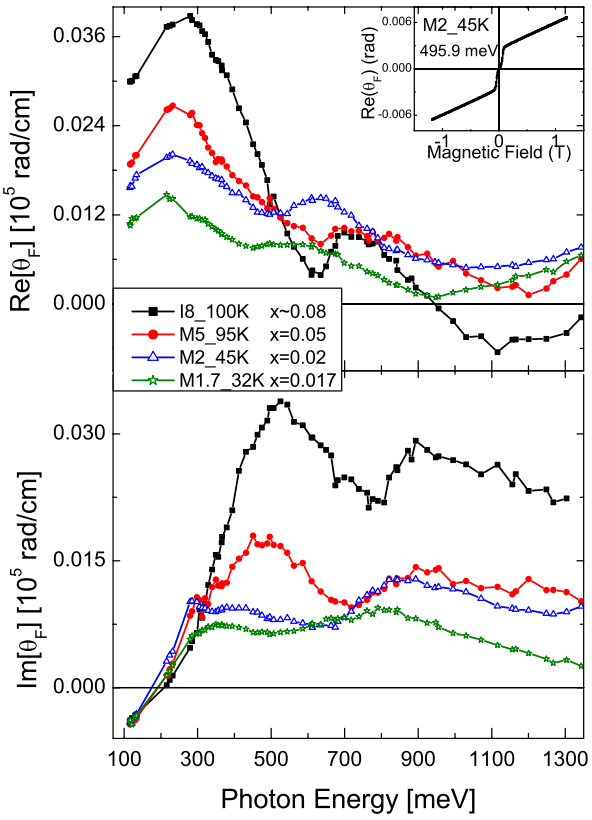

FIG. 1 (color online). Measured Faraday rotation (top) and ellipticity (bottom) vs photon energy. Top inset: $\mathrm{Re}(\theta_F)$ vs magnetic field for sample M2_45K measured at a photon energy of 495.9 meV and $T = 10$ K.

We have studied four $Ga_{1-x}Mn_xAs$ films with different ferromagnetic properties. The sample M5_95K was grown by low temperature molecular beam epitaxy on a GaAs substrate. The $Ga_{1-x}Mn_xAs$ film is 50 nm thick with a uniform nominal Mn doping of 5%, a Curie temperature $T_c = 95$ K, and a hole density $p \sim 2 \times 10^{20}$ cm^{-3} estimated from transport measurements. Sample M2_45K consists of a 50 nm thick $Ga_{1-x}Mn_xAs$ film with nominal Mn doping of 2%, $T_c = 45$ K, and $p \sim 1.5 \times 10^{20}$ cm^{-3}, and the third low temperature molecular beam epitaxy sample M1.7_32K has a 100 nm thick $Ga_{1-x}Mn_xAs$ with nominal Mn doping of 1.7%, $T_c = 32$ K, and $p \sim 1 \times 10^{20}$ cm^{-3}. Sample I8_100K was grown by ion implantation and laser pulsed melting and has $T_c \approx 100$ K and a Gaussian-like distribution of Mn ions with an estimated mean concentration of Mn of ~8% and $p \sim 4 \times 10^{20}$ cm^{-3}. Except sample I8_100K, all samples where annealed at 200 °C for 1 h.

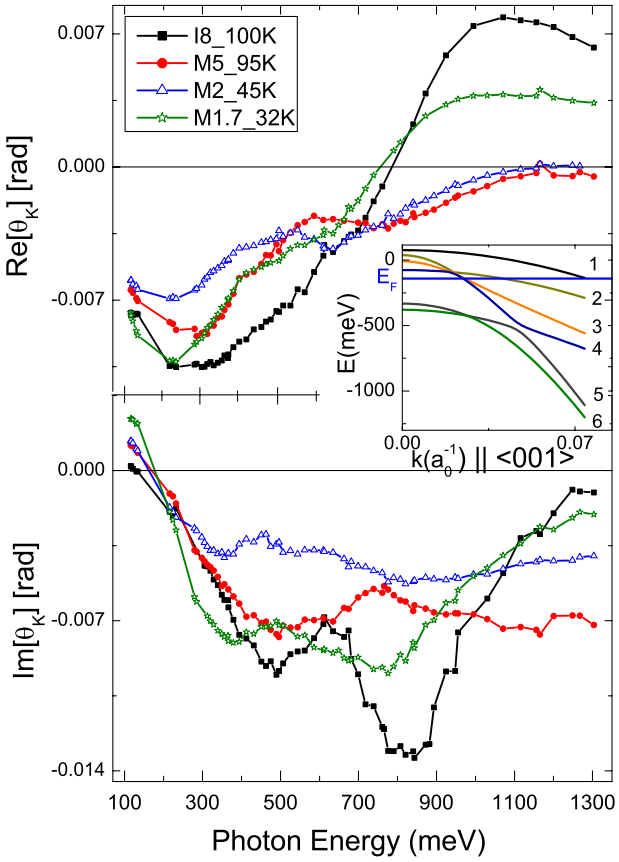

FIG. 2 (color online). Measured Kerr rotation (top) and ellipticity (bottom) vs photon energy. Inset: valence-band dispersion for $k \parallel \langle 001 \rangle$; $x = 0.05$ and 2.5×10^{20} cm^{-3}; the Fermi level is shown with a horizontal line.

The spectral dependence of the Faraday and Kerr rotation [Re(θ_F) and Re(θ_K)] and ellipticity [Im(θ_F) and Im(θ_K)] taken at 10 K are shown in Figs. 1 and 2. All samples present a similar resonant behavior. Unlike the infrared absorption which is proportional to the longitudinal conductivity σ_{xx} [9], θ_F and θ_K follow the behavior of the off-diagonal component σ_{xy}, thus exhibiting relatively sharp (~150 meV) spectral features and sign changes. The magnitude of the Faraday rotation and ellipticity grows with Mn concentration. The rotation spectra are characterized by two extrema separated by about 400 meV and a dip or sign change as the band-gap energy is approached. The ellipticity changes sign in the 200 meV region and has two maxima at higher energy. We note that features in the rotation are correlated to features in the ellipticity due to the Kramers-Kronig relations.

In the following we compare the measurements with predictions of the theory in which holes reside in an As p-orbital-dominated valence band which is coupled to Mn d-orbital local moments by an antiferromagnetic kinetic-exchange interaction [6]. The coupling is treated within the mean-field theory, and disorder is introduced through a finite lifetime broadening of the valence-band states [27,28]. We use the eight-band $\mathbf{k} \cdot \mathbf{p}$ model which takes into account the complex band structure of the valence band in the presence of the kinetic-exchange field and spin-orbit coupling (the valence-band dispersion for one direction in k space is shown in the inset in Fig. 2), as well as valence-conduction band transitions. The relatively large carrier doping also leads to band-renormalization effects [33–35] which can modify the band gap and inter-valence-band splittings. Whereas electron-electron interactions' contributions from the exchange and correlation effects tend to shift rigidly the valence and conduction bands towards each other, the impurity scattering from the randomly distributed Mn acceptors leads to a more strongly momentum dependent shift which renormalizes the inter-valence-band splittings [34,35]. We have incorporated this in the calculations by shifting rigidly the majority bands only (largest k_F) by $10 \times (p[10^{18}\ \text{cm}^{-3}])^{1/3}$ meV [34,35].

We use the calculated complex conductivities σ_{xx} and σ_{xy} in the transmission and reflection formulas for our geometry (thin film on a wedged substrate with multiple reflection effects taken into account) [31] to determine the complex θ_F and θ_K. Because of the low σ_{xx} values in these samples, θ_F and θ_K practically follow σ_{xy} and $-\sigma_{xy}$, respectively.

In Fig. 3 we plot the calculated Kerr and Faraday rotation (top panels) and ellipticity (middle panels) as a function of the photon energy for a fixed density of carriers $p = 2.0 \times 10^{20}$ cm^{-3} and varying Mn_{Ga} doping. For a fixed Mn_{Ga} doping of 5% and varying hole concentration

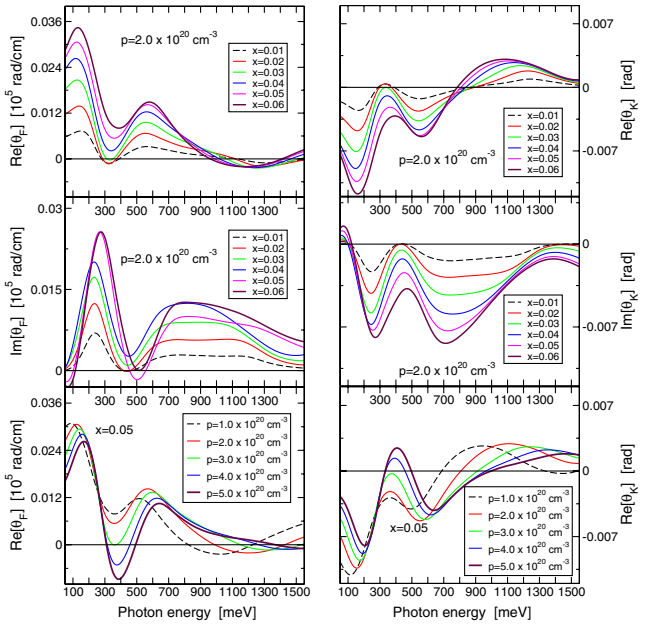

FIG. 3 (color online). Calculated Faraday rotation Re(θ_F) and ellipticity Im(θ_F) (left panels) and Kerr rotation Re(θ_K) and ellipticity Im(θ_K) (right panels) vs photon energy for samples of 50 nm thickness. Upper and middle panels show the rotation and ellipticity for several Mn_{Ga} dopings at fixed hole density, respectively. The bottom panels show the rotation for several hole densities at fixed Mn_{Ga} doping.

(bottom panels) we only show the Faraday and Kerr rotation. The strong disorder present in the experimental films is taken into account through a finite lifetime broadening of 100 meV [6,35]. The Faraday rotation has an extremum in the 150–200 meV, while the ellipticity changes sign in this region. These spectral features are due to the transitions from the light-hole to the heavy-hole originating bands (1, 2, 3, 4 in Fig. 2 inset). Contributions from the split-off originating bands (5, 6 in Fig. 2 inset) to the light-hole bands (3, 4) and the split-off bands to the heavy-hole band (1, 2) dominate the Kerr and Faraday spectra at energies higher than 500–650 meV. Our calculations capture the measured order of magnitude of the Faraday rotation angle, the separation of the two maxima, and the increase of the angle with increasing Mn_{Ga} concentration. Variations in the carrier concentration do not affect the magnitude of the Faraday angle as strongly (see lower left panel in Fig. 3).

The Faraday angle calculations also capture the dip (and a possible change in sign) of the measured $\mathrm{Re}(\theta_F)$ as the energy approaches the band gap. Kerr angle calculations (right panels in Fig. 3) show a similar general agreement with the correct location of the sign change, correct order of magnitude, and a separation of the two main peaks in the negative region.

Because of the complexity of the studied materials and approximations employed in the calculations, only a semiquantitative comparison between theory and experiment is meaningful in the case of diluted magnetic semiconductors. On this level, the overall agreement of our theoretical infrared magneto-optical spectra with experiment provides strong evidence that the conventional disordered valance band theory of ferromagnetic $Ga_{1-x}Mn_xAs$ captures correctly the magnetic and orbital nature and density of states near the Fermi energy. We emphasize that our microscopic calculations use no adjustable parameters. This applies to the basic spin-splitting and orbital characteristics of the bands which we have accounted for within the $\mathbf{k}\cdot\mathbf{p}$ model antiferromangetically coupled to the localized Mn d electrons and whose similar description can be obtained using the spd-tight-binding model or LDA + U full potential density-functional calculations [6,29]. It also applies to the additional effects of disorder and interactions on the imaginary and real parts of the hole Green's function; the former has been estimated based on numerical Fermi's golden rule calculations in $Ga_{1-x}Mn_xAs$ [6] and the latter from detailed band-renormalization studies in heavily p-doped semiconductors [34,35].

In conclusion, we have presented results of Faraday and Kerr effect measurements in the subgap region in order to study the electronic structure of $Ga_{1-x}Mn_xAs$. By measuring θ_F and θ_K, which arise from transitions between exchange-split and spin-orbit coupled states, and after subtracting the paramagnetic background, we obtained spectral features corresponding to the ferromagnetically coupled electronic states near the Fermi energy. Microscopic calculations based on the conventional semiconductor valence-band picture of $Ga_{1-x}Mn_xAs$ account for the position of the main spectral features and for the Mn-concentration dependent magnitude of the measured magneto-optical signals.

This work was supported by the Research Corporation Cottrell Scholar Grant (J. C. and J. S.); NSF-CAREER-DMR0449899 (J. C.); UB CAS (J. C.); DOE Contract No. DE-AC03-76SF00098 (O. D. D.); ONR-N000140610122 (J. S. and T. J.); NSF-CAREER–DMR-0547875 (J. S.); the SWAN-NRI (J. S. and T. J.); EU Grants No. FP7-215368 SemiSpinNet and No. FP7-214499 NAMASTE; Czech Republic Grants No. FON/06/E001, No. FON/06/E002, No. AV0Z10100521, No. KAN400100652, No. LC510; and Preamium Academiae (T. J. and V. N.).

[1] H. Ohno *et al.*, Phys. Rev. Lett. **68**, 2664 (1992).
[2] T. Dietl A. Haury, Y. M. dAubigne, Phys. Rev. B **55**, R3347 (1997).
[3] H. Ohno, Science **281**, 951 (1998).
[4] T. Jungwirth *et al.*, Phys. Rev. B **59**, 9818 (1999).
[5] T. Dietl *et al.*, Science **287**, 1019 (2000).
[6] T. Jungwirth *et al.*, Rev. Mod. Phys. **78**, 809 (2006).
[7] V. Novák *et al.*, Phys. Rev. Lett. **101**, 077201 (2008).
[8] *Spintronics*, edited by T. Dietl, D. D. Awschalom, M. Kaminska, and H. Ohmo, Semiconductors and Semimetals Vol. 82 (Elsevier, New York, 2008).
[9] K. S. Burch *et al.*, Phys. Rev. Lett. **97**, 087208 (2006).
[10] T. Jungwirth *et al.*, Phys. Rev. B **76**, 125206 (2007).
[11] L. P. Rokhinson *et al.*, Phys. Rev. B **76**, 161201(R) (2007).
[12] I. Garate *et al.*, Phys. Rev. B **79**, 155207 (2009).
[13] P. R. Stone *et al.*, Phys. Rev. Lett. **101**, 087203 (2008).
[14] J.-M. Tang and M. E. Flatté, Phys. Rev. Lett. **101**, 157203 (2008).
[15] K. Ando *et al.*, Phys. Rev. Lett. **100**, 067204 (2008).
[16] V. Holý *et al.*, Phys. Rev. B **74**, 245205 (2006).
[17] M. A. Scarpulla *et al.*, Appl. Phys. Lett. **82**, 1251 (2003).
[18] M. A. Scarpulla *et al.*, J. Appl. Phys. **103**, 073 913 (2008).
[19] K. Ando *et al.*, J. Appl. Phys. **83**, 6548 (1998).
[20] T. Kuroiwa *et al.*, Electron. Lett. **34**, 190 (1998).
[21] B. Beschoten *et al.*, Phys. Rev. Lett. **83**, 3073 (1999).
[22] J. Szczytko *et al.*, Phys. Rev. B **59**, 12 935 (1999).
[23] R. Lang *et al.*, Phys. Rev. B **72**, 024430 (2005).
[24] R. Chakarvorty *et al.*, Appl. Phys. Lett. **91**, 171118 (2007).
[25] T. Komori *et al.*, Phys. Rev. B **67**, 115203 (2003).
[26] T. Jungwirth *et al.*, Appl. Phys. Lett. **83**, 320 (2003).
[27] J. Sinova *et al.*, Phys. Rev. B **67**, 235203 (2003).
[28] E. M. Hankiewicz *et al.*, Phys. Rev. B **70**, 245211 (2004).
[29] J. Masek *et al.* (unpublished).
[30] J. Cerne *et al.*, Rev. Sci. Instrum. **74**, 4755 (2003).
[31] M.-H. Kim *et al.*, Phys. Rev. B **75**, 214416 (2007).
[32] M.-H. Kim *et al.*, arXiv:0907.3128.
[33] K. F. Berggren and B. E. Sernelius, Phys. Rev. B **24**, 1971 (1981).
[34] B. E. Sernelius, Phys. Rev. B **34**, 5610 (1986).
[35] Y. Zhang and S. Das Sarma, Phys. Rev. B **72**, 125303 (2005).